

## NRC Publications Archive Archives des publications du CNRC

### Renewable energy system demonstration at CHARS: modelling analysis report

Wills, Adam D.; Falconer, Alix; Banister, Carsen; Vuotari, Mark

For the publisher's version, please access the DOI link below./ Pour consulter la version de l'éditeur, utilisez le lien DOI ci-dessous.

<https://doi.org/10.4224/40003943>

#### NRC Publications Archive Record / Notice des Archives des publications du CNRC :

<https://nrc-publications.canada.ca/eng/view/object/?id=185ec870-730f-43ce-8860-f93b7fb31b0d>

<https://publications-cnrc.canada.ca/fra/voir/objet/?id=185ec870-730f-43ce-8860-f93b7fb31b0d>

Access and use of this website and the material on it are subject to the Terms and Conditions set forth at

<https://nrc-publications.canada.ca/eng/copyright>

READ THESE TERMS AND CONDITIONS CAREFULLY BEFORE USING THIS WEBSITE.

L'accès à ce site Web et l'utilisation de son contenu sont assujettis aux conditions présentées dans le site

<https://publications-cnrc.canada.ca/fra/droits>

LISEZ CES CONDITIONS ATTENTIVEMENT AVANT D'UTILISER CE SITE WEB.

**Questions?** Contact the NRC Publications Archive team at

PublicationsArchive-ArchivesPublications@nrc-cnrc.gc.ca. If you wish to email the authors directly, please see the first page of the publication for their contact information.

**Vous avez des questions?** Nous pouvons vous aider. Pour communiquer directement avec un auteur, consultez la première page de la revue dans laquelle son article a été publié afin de trouver ses coordonnées. Si vous n'arrivez pas à les repérer, communiquez avec nous à PublicationsArchive-ArchivesPublications@nrc-cnrc.gc.ca.

**CONSTRUCTION**

# Renewable Energy System Demonstration at CHARS

## Modelling Analysis Report

Author(s): Adam D. Wills, Alix Falconer, Carsen  
Banister, Mark Vuotari

Report No.: A1-019271.01

Report Date: 16 June 2022

Contract No.: A1-019271

Agreement Date: 15 March 2021



National Research  
Council Canada

Conseil national de  
recherches Canada



Polar Knowledge  
Canada

Savoir polaire  
Canada



# Renewable Energy System Demonstration at CHARs

## Modelling Analysis Report

Author **Wills,  
Adam** Digitally signed by Wills, Adam  
DN: cn=Wills, Adam, c=CA, o=GC,  
ou=NRC-CNRC,  
email=adam.wills@cnrc-nrc.gc.ca  
Date: 2022.07.05 13:38:20 -04'00'

---

Adam D. Wills, Ph.D.

Approved **Gover,  
Bradford** Digitally signed by Gover,  
Bradford  
DN: cn=Gover, Bradford, c=CA,  
o=GC, ou=NRC-CNRC,  
email=brad.gover@canada.ca  
Date: 2022.09.09 12:24:54 -04'00'

---

Bradford Gover, Ph.D.  
Director, Research and Development  
Building Envelope and Materials,  
Intelligent Building Operations  
NRC Construction Research Centre

Report No: A1-019271.01  
Report Date: 16 June 2022  
Contract No: A1-019271  
Agreement date: 15 March 2021  
Program: IBO R&D

32 pages

Copy no. 1 of 3

This report may not be reproduced in whole or in part without the written consent of the National Research Council Canada and the Client.

# Renewable Energy System Demonstration at CHARs

## Modelling Analysis Report

Author **Wills,  
Adam** Digitally signed by Wills, Adam  
DN: cn=Wills, Adam, c=CA, o=GC,  
ou=NRC-CNRC,  
email=adam.wills@cnrc-nrc.gc.ca  
Date: 2022.07.05 13:38:46 -04'00'

---

Adam D. Wills, Ph.D.

Approved **Gover,  
Bradford** Digitally signed by Gover,  
Bradford  
DN: cn=Gover, Bradford, c=CA,  
o=GC, ou=NRC-CNRC,  
email=brad.gover@canada.ca  
Date: 2022.09.09 12:25:06 -04'00'

---

Bradford Gover, Ph.D.  
Director, Research and Development  
Building Envelope and Materials,  
Intelligent Building Operations  
NRC Construction Research Centre

Report No: A1-019271.01  
Report Date: 16 June 2022  
Contract No: A1-019271  
Agreement date: 15 March 2021  
Program: IBO R&D

32 pages

Copy no. 2 of 3

This report may not be reproduced in whole or in part without the written consent of the National Research Council Canada and the Client.

# Renewable Energy System Demonstration at CHARs

## Modelling Analysis Report

Author **Wills,  
Adam** Digitally signed by Wills, Adam  
DN: cn=Wills, Adam, c=CA, o=GC,  
ou=NRC-CNRC,  
email=adam.wills@cnrc-nrc.gc.ca  
Date: 2022.07.05 13:38:57 -04'00'

---

Adam D. Wills, Ph.D.

Approved **Gover,  
Bradford** Digitally signed by Gover,  
Bradford  
DN: cn=Gover, Bradford, c=CA,  
o=GC, ou=NRC-CNRC,  
email=brad.gover@canada.ca  
Date: 2022.09.09 12:25:14 -04'00'

---

Bradford Gover, Ph.D.  
Director, Research and Development  
Building Envelope and Materials,  
Intelligent Building Operations  
NRC Construction Research Centre

Report No: A1-019271.01  
Report Date: 16 June 2022  
Contract No: A1-019271  
Agreement date: 15 March 2021  
Program: IBO R&D

32 pages

Copy no. 3 of 3

This report may not be reproduced in whole or in part without the written consent of the National Research Council Canada and the Client.

*(This page is intentionally left blank)*

# Table of Contents

Table of Contents.....	i
List of Figures .....	iii
List of Tables .....	iv
Executive Summary .....	v
1 Introduction.....	1
2 Methodology .....	1
Model Overview .....	2
2.2 Model Components.....	2
2.2.1 Climate .....	2
2.2.2 Wind Turbine .....	2
2.2.3 Battery .....	3
2.2.4 Diesel Generator.....	4
2.2.5 Grid Controller .....	5
2.2.6 Equipment Sheds .....	7
2.2.7 Photovoltaics .....	9
System Loads.....	10
2.3.1 Vehicle Block Heaters.....	10
2.3.2 Facility Lights.....	10
2.3.3 Facility Garage Door.....	11
2.3.4 Standby Loads.....	11
2.4 Performance Metrics.....	11
3 Simulation Cases.....	13
Battery Size Variation .....	13
3.2 Integration of Solar PV.....	13
Load Sensitivity.....	13
4 Results.....	15
4.1 Baseloads.....	15
Base Case System Performance .....	17
4.3 Battery Capacity Study .....	19
Solar PV Study .....	21
4.4.1 Site Solar Resource Study.....	21

4.4.2	PV Integration into System .....	23
	Baseload Sensitivity Study.....	25
4.5.1	Scenario B: Quadrupled Block Heater Loads.....	25
4.5.2	Scenario C: Doubled Block Heater Loads.....	26
5	Discussion .....	28
6	Conclusions .....	29
7	Acknowledgements.....	30
8	References .....	31

## List of Figures

Figure 1. CHARS site in Cambridge Bay, Nunavut.....	1
Figure 2. CHARS TRNSYS renewable generation model .....	2
Figure 3. SD6 wind turbine power output versus wind speed at hub, data from ICC-SWCC (2019) .....	3
Figure 4. Diesel generator part-load versus fuel consumption, based on data from Hatz Diesel (2020) .....	4
Figure 5. Micro-grid configuration and energy flow assumed by controller .....	6
Figure 6. Rendering of Type 56 equipment shed models .....	8
Figure 7. Resistor-diode PV model schematic, adapted from De Soto et al. (2006) .....	9
Figure 8. PV panel azimuth and slope angle definitions .....	13
Figure 9. Daily electrical demand profile, excluding space heating.....	15
Figure 10. Simulated space heating electrical demand for first week of January .....	15
Figure 11. Site demands load-duration curve .....	16
Figure 12. Base renewable system annual energy flow.....	17
Figure 13. Base system monthly energy balance .....	18
Figure 14. Base system load, generation, and battery state-of-charge duration curves.....	19
Figure 15. Double battery capacity system annual energy flow .....	20
Figure 16. Annual PV module production parametric study .....	21
Figure 17. Monthly PV module production at optimal point.....	22
Figure 18. Variation of PV seasonal production curve and slope.....	22
Figure 19. Variation of PV daily production curve and azimuth for month of July.....	23
Figure 20. Annual energy flow of base system with integrated PV .....	24
Figure 21. System with integrated PV monthly energy balance .....	25
Figure 22. Load scenario B annual system energy flow .....	26
Figure 23. Load scenario C annual system energy flow .....	27
Figure 24. Average daily wind generation profile.....	28

## List of Tables

Table 1. Summary of wind turbine model parameters .....	3
Table 2. Summary of battery model parameters.....	4
Table 3. Summary of diesel generator model parameters .....	5
Table 4. Summary of grid controller model parameters .....	7
Table 5. Summary of equipment sheds envelopes.....	8
Table 6. Summary of PV module model parameters, based on data from Canadian Solar (2018) .....	10
Table 7. Summary of emission factors from diesel combustion .....	12
Table 8. Summary of base system system annual performance metrics .....	18
Table 9. Comparison of double battery capacity and base system annual performance metrics .....	20
Table 10. Comparison of integrated PV and base system annual performance metrics .....	24
Table 11. Comparison of base and integrated PV systems monthly diesel generation .....	25
Table 12. Impact of increased block heating loads (Scenario B) on base system performance.	26
Table 13. Impact of increased block heating loads (Scenario C) on base system performance.	27

## Executive Summary

The majority of the energy demands in the Canadian Arctic are met with fossil fuels such as heating oil and diesel electric generation. As a result of climate change impacts, there is strong desire to explore and adopt renewable electricity generation technologies. There is also a desire to increase resilience of energy infrastructure, not just in the Arctic, but globally. The Arctic presents unique challenges in deploying renewable generation technologies due to the unique environmental conditions, logistics, and policies.

This project is focused on the deployment of a small wind turbine and battery energy storage system for an off-grid energy system primarily to meet the lighting and vehicle block heating loads of a large storage shelter located at the Canadian High Arctic Research Station in Cambridge Bay, Nunavut. Polar Knowledge Canada operates and manages the facility, and is collaborating with National Research Council Canada on the project. The energy system will be instrumented and monitored to evaluate the performance of the turbine under Arctic operating conditions. This is the first report issued for the project, which describes the simulation and analysis of the system undertaken by NRC to support equipment selection and system design.

Wind is a renewable energy resource which is typically available throughout the year and likely to be a more consistent source to meet energy demands in the Arctic, whereas solar energy has significant seasonal variation at high latitudes. Several wind demonstration projects have been undertaken in Nunavut since the 1990s, but these have been short-lived due to high maintenance costs and equipment failure under harsh Arctic conditions. Nonetheless, the technology has continued to advance over the past few decades and it is of interest to determine if the latest generation of wind turbine technologies can reliably utilize available wind resources.

The micro-grid system was modelled using the transient energy system simulation tool TRNSYS. The performance of a 6 kW commercially-available wind turbine was simulated using manufacturer-reported performance data and climate data for Cambridge Bay provided by Environment and Climate Change Canada. A transient model of a 22.8 kWh battery system was also implemented into the model, as well as an empirical model of a diesel generation system and numerical models of the equipment shelters.

The simulation analysis estimated that the renewable energy system will reduce annual greenhouse gas emissions by 21%. An additional simulation showed that doubling the specified battery capacity increased annual emissions reductions by 31%. The potential benefit of including on-site solar generation was also analyzed by adding a 2.32 kW solar PV array to the base system model, and it was shown to achieve annual emissions reductions by 46%. This PV study highlighted that despite the significant seasonal variation and demand-generation mismatch associated with solar in the Arctic, there is still a potential for significant benefit from solar PV dispatched in Arctic climates.

Finally, the sensitivity of the micro-grid system performance to demand estimates was analyzed by doubling and quadrupling annual energy demand for vehicle block heating. These loading scenarios were found to reduce annual emissions savings to 13% and 7%, respectively. These results highlighted the significant sensitivity of system performance to site demand characteristics.

# 1 Introduction

Renewable energy from wind and solar as a sustainable means to meet energy needs in the Arctic has had historic interest, but only recently growing success. Equipment designed for and able to withstand the high winds, extreme cold, and unique precipitation of the Arctic is a crucial aspect that was often overlooked. Capacity to operate and maintain the equipment in a remote community is also crucial to success. Wind turbines have been installed in the past in some Arctic locations, such as Cambridge Bay, but have not had a successful operational life due to these factors and more. Technology, capabilities, and interest has advanced over the intervening years, but due to the very challenging environment, installation and testing must still be approached with care and from a perspective of research and development. In other words, like many technologies, renewable energy system composed of wind and solar generation are in the initial stages of utilization in Canada's Arctic and much is still to be learned as they function over their planned lifecycle through the application of appropriate measuring, monitoring, maintenance, analysis, and advancement of design.

This report details the simulation work that was undertaken to estimate the performance and operation of a micro-grid system to be installed at the Canadian High Arctic Research Station (CHARS) located in Cambridge Bay, with the general site shown in Figure 1. The system is to contain a single wind turbine generator coupled with battery storage to supply energy to lighting, block heating, and space heating of an equipment shelter. The purpose of this study was to estimate and analyze the potential greenhouse gas emissions reductions that may be realized by the system, the potential benefits of additional battery capacity and solar photovoltaic generation integration, and the sensitivity of system performance to site demand characteristics.



Figure 1. CHARS site in Cambridge Bay, Nunavut

## 2 Methodology

Analysis of the proposed renewable generation system was conducted using the energy system simulation tool TRNSYS (TESS, 2019a). TRNSYS was initially developed as a simulation tool for solar thermal systems (Klein, et al., 1975), and its capabilities have been extended to include the dynamic simulation of a variety of energy transfer and conversion systems. The smallest functional unit in a TRNSYS model is a "Type." A Type is a subroutine which models the static and dynamic characteristics of a system component. The Type is supplied with a set of static parameters at initialization, such as component scales and characteristics, and receives inputs and calculates outputs in a user-defined network of Types.

TRNSYS is pre-packaged with libraries of Types that include a variety of energy transfer and conversion system components with varying model complexities; some Types represent simple components like pipes and fans, while others represent entire co-generation plants. Since TRNSYS is an open-source tool, additional Types may be developed to meet the needs of the user.

## 2.1 Model Overview

The TRNSYS model developed for the proposed renewable generation system is illustrated in Figure 2.

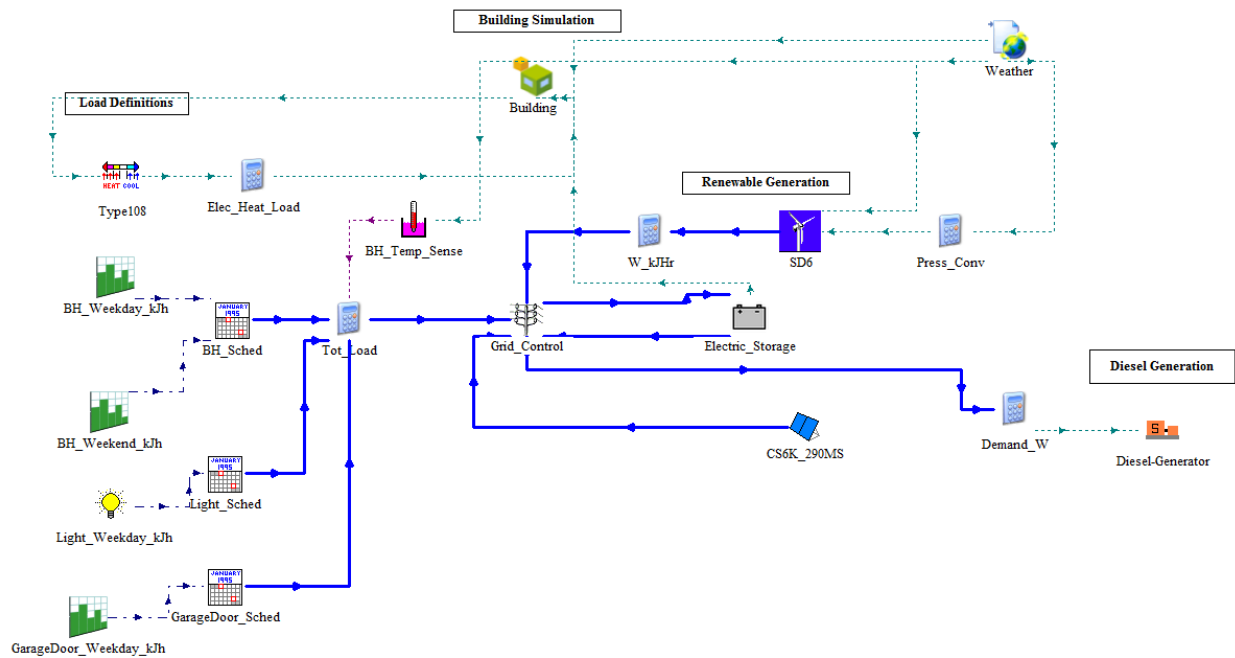


Figure 2. CHARS TRNSYS renewable generation model

Central to the model is the grid controller Type, labelled “Grid\_Control” in Figure 2. This was a custom TRNSYS Type developed for this work to model the management of the CHARS micro-grid. The controller monitors the electrical demands on the system, described later in Section 2.3, and manages the charge/discharge of the battery, dispatch of the on-site diesel generator, and wind generation output. The following subsections provide descriptions of the principal system Types used in the model.

## Model Components

### 2.2.1 Climate

TRNSYS standard library Type 15 (TESS, 2019b) was used to load annual climate data into the model; shown in Figure 2 as “Weather”. For this simulation study, the annual hourly Canadian Weather Year for Energy Calculations (CWEC) data file for Cambridge Bay, NU from Environment and Climate Change Canada (ECCC, 2021a) was used. Drybulb temperature, relative humidity, and wind speed and direction are linearly interpolated by Type 15 to determine sub-hourly conditions. Sub-hourly solar radiation is processed using the hourly solar intensity values available in the climate file and solar processing algorithms provided in Duffie & Beckman (2006) to determine solar angles at each sub-hourly timestep.

### 2.2.2 Wind Turbine

The wind turbine was modelled using TRNSYS standard library Type 90 (TESS, 2019b), labelled as “SD6” in Figure 2. Type 90 is an empirical steady-state model which uses manufacturer reported test data to model turbine power output and performance under different environmental operating conditions. The power versus output curve under standard testing conditions forms the primary model for the turbine. The SD6 wind turbine from SD Wind Energy was considered for installation at CHARS and its characteristics were implemented into the model.

The SD6 turbine is a three-blade horizontal axis turbine with a swept area of 23.7 m<sup>2</sup>. Standard test data for the SD6 turbine was obtained from the Small Wind Certification Council (ICC-SWCC, 2019). Figure 3 plots the turbine power output versus wind speed at the hub height from ICC-SWCC (2019). The curve represents performance with a turbine inlet air density of 1.225 kg/m<sup>3</sup>.

Figure 3. SD6 wind turbine power output versus wind speed at hub, data from ICC-SWCC (2019)

The Type 15 climate processing component provides the wind speed, ambient drybulb temperature, and barometric pressure boundary conditions to the wind turbine model for each simulation timestep. Table 1 provides a summary of the wind turbine model parameters.

Table 1. Summary of wind turbine model parameters

Parameter	Value
Rotor height [m]	9.0
Rotor diameter [m]	5.6
Rated power [kW]	5.2
Rated wind speed [m/s]	11.0

Additional details of the wind turbine modelling methodology are omitted here for clarity, and the interested reader is directed to TESS (2019b) for additional information.

### 2.2.3 Battery

The battery system was modelled using TRNSYS standard library Type 47 (TESS, 2019b), illustrated in Figure 2 as “Electric\_Storage”. There are various sub-algorithms available of this Type which provide greater model detail at the expense of additional parameter inputs. For the purposes of this study, the base transient energy balance algorithm was used. This approach uses a basic in, out, and stored energy balance approach to model the battery.

To account for battery energy transfer and storage inefficiencies, Type 47 has a constant charging efficiency input parameter. This parameter is applied as energy is passed into the battery; e.g. if efficiency is 90%, then only 90% of the power directed to the battery will be stored in the battery and the remaining 10% is taken as losses due to inefficiencies. During discharge, however, the model simply subtracts the requested energy from the battery without applying any discharge losses. In practice, there are energy losses in batteries associated with charge, discharge, and self-discharge during idle. To account for all these loss mechanisms in the model, the charging efficiency parameter is typically defined such that it reflects the “round-trip” efficiency; i.e. the fraction of energy directed to the battery that can be recovered during discharge, accounting for all losses during charge,

idle, and discharge operation phases. Type 47 likely uses this “loss at charge time only” approach to simplify the simulation of transient operation and control of the battery system.

For this study, a baseline battery bank size of 22.8 kWh was considered. This value was based on a battery bank of six 3.8 kWh lithium ferro phosphate batteries (SimpliPhi Power, 2022). Given the simplicity of the model, it may be considered battery technology type agnostic. The charging efficiency was assumed to be 90% based on assumed round-trip efficiency of lithium-ion batteries reported by Brown (2018). The key battery model parameters are summarized in Table 2.

Table 2. Summary of battery model parameters

Parameter	Value
Cell energy capacity [Wh]	3800
Cells in parallel	6
Cells in series	1
Charging efficiency [%]	90.0

Further details of the battery model are omitted here for clarity, and the interested reader is directed to TESS (2019b) for additional information.

It was assumed that the battery and various micro-grid system components were housed in an electrical shed, and that losses from battery charging are passed as thermal gains to the enclosure. The electrical system enclosure was explicitly modelled, and is described in Section 2.2.6.

### 2.2.4 Diesel Generator

The diesel generation system was modelled using TRNSYS standard library Type 120 (TESS, 2019b), shown in Figure 2 as “Diesel-Generator”. Type 120 is a steady-state empirical performance map model constructed around a part-load ratio to fuel consumption rate curve. Based on input from project partners, a 7.6 kW<sub>e</sub> diesel generation system (Hatz Diesel, 2020) was tentatively planned for the site. This generator’s performance curve is plotted in Figure 4.

Figure 4. Diesel generator part-load versus fuel consumption, based on data from Hatz Diesel (2020)

The manufacturer reported fuel consumption, in grams per kWh, versus electrical power output. Type 120, however, requires the performance curve to be characterized using the units provided in Figure 4. To convert gram of fuel per kWh to litres per hour a diesel fuel density of 833 grams per litre was assumed. This value is

taken from ISED (2018) for diesel fuel at 25 °C, which is the ambient temperature reported by the manufacturer for test conditions.

It can be seen in Figure 4 that the performance curve can be accurately approximated using a linear regression, with a coefficient of determination,  $R^2$ , of 0.99. While a second-order polynomial was found to more precisely capture the manufacturer reported data points in Figure 4, the model implementation is limited to linear expressions of performance curves.

The salient model parameters are summarized in Table 3.

Table 3. Summary of diesel generator model parameters

Parameter	Value
Maximum electrical generation capacity [kW]	7.9
Minimum electrical generation capacity [kW]	3.9
Rated electrical generation [kW]	7.6
Performance curve slope [g/litre/PLR]	2.777
Performance curve intercept [g/litre]	-0.356

Operation of the diesel generator is governed by the grid controller, described in section 2.2.5. For each time step, the controller passes a power demand to the diesel generator. If this demand is below the minimum operating threshold of the generator, the generator operates at its minimum output capacity and excess electrical generation is directed by the grid controller to either the battery charging system or, if the batteries are fully charged, to an electrical dump load. Similarly, if requested generation exceeds maximum generator capacity, the generator operates at its maximum capacity point and additional energy is assumed to be drawn from the local utility grid.

The diesel generator is assumed to be housed in an enclosure which is a separate structure from the enclosure housing the electrical system. This enclosure was explicitly modelled, and is described in section 2.2.6. Similar to the battery model, a portion of thermal losses from the generator are passed to the enclosure as thermal energy gains. It was assumed that 44.4% of thermal losses of the generator were passed to the enclosure, and the remaining 55.6% was vented directly outside in the exhaust stream. These values were based on estimates reported by Brown (2018) for diesel gensets.

## 2.2.5 Grid Controller

Basic and fit-for-purpose grid control types were currently available in the TRNSYS standard and extended libraries. It was identified that for the current application, however, a new Type was needed to manage the modelled energy system shown in Figure 2. The new control Type was designed to meet the needs of the current modelling study, but also be generic enough such that it can be deployed in future micro-grid simulation research studies. Figure 5 illustrates what the new micro-grid controller Type assumes for the structure of the micro-grid and the components it can control.

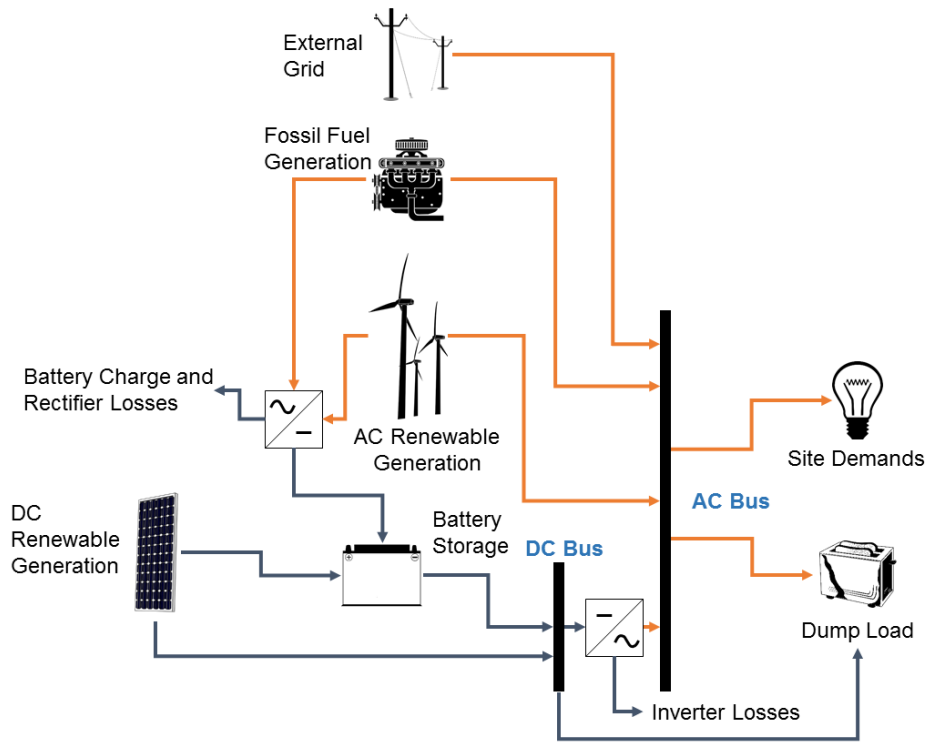


Figure 5. Micro-grid configuration and energy flow assumed by controller

Shown as “Grid\_Controller” in Figure 2, this new TRNSYS Type acts as the central hub of the system energy model. At each simulation time step, AC and DC electricity generation, battery state-of-charge (SOC), and total site AC demand are taken as inputs to the controller to determine dispatch and control action. The grid controller also models the performance of the DC-to-AC inverter and AC-to-DC rectifier in Figure 5. Both devices are modelled assuming user-prescribed constant conversion efficiencies.

The primary priority of the control algorithm was to first supply all on-site renewable generation to concurrent site energy demands. This choice was made because on-site generation is best utilized by directly supplying concurrent site demands rather than storing it for later use which incurs charge, discharge, and standby losses in the system. If there is insufficient or no available renewable generation during a period of site demand, the battery is then discharged if there is sufficient capacity available. Battery capacity is determined by the battery’s SOC, and also by a maximum battery power draw limit specified by the user. If there is insufficient capacity from the battery to meet the site loads, the battery is dispatched to provide as much power it is able to deliver at that time, and if there is any remaining site demand the controller dispatches the diesel generation system.

Stated previously in Section 2.2.4, the diesel generator can only operate between its maximum and minimum power outputs. The grid controller model was designed such that it is aware of these limitations and their values. Therefore, if remaining site demand to be met is greater than the capacity of the generator, the controller accounts for this deficit by dispatching the generator to output and maximum load having the remainder of the load met by the external utility grid. Conversely, if remaining site demand after renewable generation and battery systems have been dispatched is below the minimum operating point of the generator, the controller dispatches the diesel generator to operate at its minimum point and the surplus generation is passed to the battery system, illustrated as the connection between the fossil fuel generator and battery system via the rectifier in Figure 5.

During periods of excess generation, i.e. where there is less demand than generation and batteries are fully charged, surplus power is directed from the DC and/or AC buses to a dump load. In practice this dump load could

be a resistive dump load device, a diversion load, or instead be curtailment of on-site renewable generation systems outputs.

The controller Type input parameters are summarized in Table 4.

Table 4. Summary of grid controller model parameters

Parameter	Value
High limit of battery SOC [%]	98
Low limit of battery SOC [%]	20
Battery output power capacity [kW]	10.8
Charge SOC threshold [%]	N/A
Inverter efficiency [%]	95
Rectifier efficiency [%]	95

The grid controller maintains a range of battery bank SOC based on the high and low limits described in Table 4. The high limit of 98% was implemented instead of 100% to promote numerical convergence in the model. The low limit of 20% was selected to reflect the 80% depth-of-discharge (DoD) used by the manufacturer (SimpliPhi Power, 2022) when they rated the cycle life of the battery. Battery power output capacity was estimated by multiplying the manufacturer reported maximum continuous charge/discharge rate of 37.5 Amps (SimpliPhi Power, 2022) by 48 Volts, and multiplying the product by six (number of batteries in parallel) to yield 10.8 kW. Per electrical schematics provide by Polar Knowledge Canada the battery bank is connected to a 48 V DC bus.

The charge SOC threshold was a parameter implemented in the control algorithm to include functionality present in the TRNSYS standard library grid controller Type 48. While not used in this simulation, this threshold can specify a limit where if the battery bank is below the SOC threshold and starts charging, then it must continue charging until the SOC of the battery meets the threshold. Otherwise if the battery bank is discharging and passes below the threshold, it can keep discharging to its low limit of battery SOC. This enables an additional limit on deep discharge of the battery while still making capacity available during high periods of demand.

## 2.2.6 Equipment Sheds

The micro-grid system is assumed to contain two equipment sheds which are used to house generation system components: one shed houses the battery and grid control systems, and the other houses the diesel generation system. Both sheds are assumed to be constructed from standard 10 foot shipping containers, and were modelled in TRNSYS using Type 56 (TESS, 2019c). This is a detailed multi-zone building energy model that is included as a standard library component with TRNSYS. Detail of the calculation methodology of Type 56 are omitted here for clarity, and the interested reader is directed to Stephenson & Mitalas (1971), Mitalas & Arseneault (1972), and TESS (2019c) for further information. Figure 6 illustrates the model rendering of the sheds.

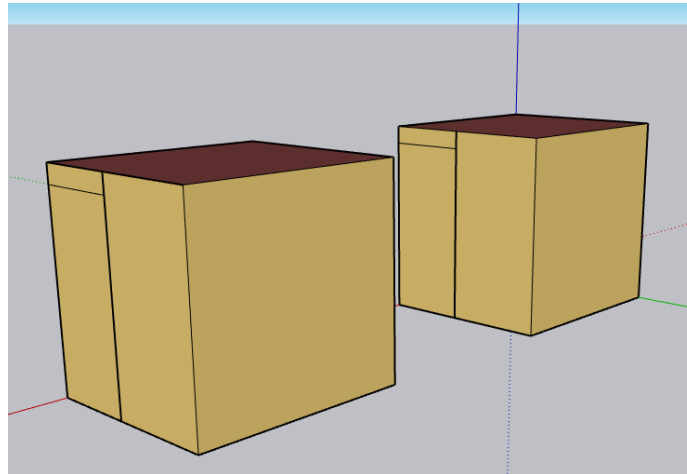


Figure 6. Rendering of Type 56 equipment shed models

The internal dimensions of each shed were initially specified as 2.66 m by 2.35 m by 2.38 m height to conform to typical 10' shipping container dimensions (Northern Container, 2022). A 0.91 m by 2.0 m access door was modelled for each shed on their eastern façades, shown as the vertical rectangular surfaces in Figure 6. The walls and roofs were modelled as being insulated with 6 inches (152.4 mm) of polyisocyanurate (PIR) with 2 mm of sheet steel cladding. The internal dimensions of the shed were reduced in the model to reflect the addition of PIR in the interior.

The access doors were assumed to be steel clad with a 2" (50.8 mm) core of extruded polystyrene (XPS). The floor was assumed to be, from exterior to interior: 2 mm steel sheet, ¾ inch (19 mm) plywood, lumber joists @ 406 mm on centre (O.C.) with R-21 batt cavity fill, ¾ inch plywood, 2 inch (50.8 mm) XPS, and terrazzo flooring. The envelope constructions for both sheds are summarized in Table 5.

Table 5. Summary of equipment sheds envelopes.

Component	Construction [Exterior to Interior]	Effective RSI [m <sup>2</sup> ·K/W]
Wall	<ul style="list-style-type: none"> <li>2 mm sheet steel</li> <li>152.4 mm PIR</li> </ul>	4.41
Roof	<ul style="list-style-type: none"> <li>2 mm sheet steel</li> <li>152.4 mm PIR</li> </ul>	4.41
Floor	<ul style="list-style-type: none"> <li>2 mm steel sheet</li> <li>19 mm plywood</li> <li>R-21 batt and lumber joists @ 406 mm O.C.</li> <li>19 mm plywood</li> <li>50.8 mm XPS</li> <li>Terrazzo flooring</li> </ul>	4.96
Door	<ul style="list-style-type: none"> <li>2 mm sheet steel</li> <li>50.8 mm XPS</li> <li>2 mm sheet steel</li> </ul>	1.69

The majority of the thermal properties of the construction materials listed in Table 5 were taken from ASHRAE Fundamentals (2009). The thermal conductivity of PIR was assumed to be 0.0362 W/(m·K) based on measured data reported by Berardi & Naldi (2017) at mean material temperature of -10.2 °C. Studies, such as those from Berardi & Naldi (2017) and Makaveckas et al. (2021), have shown that PIR thermal conductivity varies with

material temperature. Type 56 is only capable of modelling constant envelope thermophysical properties, thus a constant conductivity value based on  $-10\text{ }^{\circ}\text{C}$  was selected to reflect expected nominal operating conditions and provide a conservative estimate on insulation performance since Berardi & Naldi (2017) and Makaveckas et al. (2021) show minimal conductivity in the  $10\text{ }^{\circ}\text{C}$  to  $20\text{ }^{\circ}\text{C}$  range, and increasing conductivity outside this range. For reference, the National Building Code (NBC) (CCBFC, 2015) lists PIR as having conductivities of 0.025 to 0.028  $\text{W}/(\text{m}\cdot\text{K})$ , depending on thickness and facing of the material. PIR density and capacitance was assumed to be  $30\text{ kg}/\text{m}^3$  and  $1.5\text{ kJ}/(\text{kg}\cdot\text{K})$ , respectively, based on values reported in ASHRAE Fundamentals (2009).

The effective RSI value of the floor assemblies were determined accounting for thermal bridging through the lumber joists using the isothermal planes method as described in Section A-9.36.2.4.(1) of the 2015 NBC (CCBFC, 2015). The framing and cavity fractions for the lumber floor joists were taken from Table 9.36.2.4.(1)-A of the 2015 NBC for lumber joists with 406 mm O.C. spacing. All other effective RSI values reported in Table 5 were calculated in compliance with the 2015 NBC, but exclude the thermal resistance of the convective layers at the air boundaries. The air boundary layer resistances are calculated separately in Type 56, and were specified in the model to comply with assumptions listed in Table A-9.36.2.4.(1)-D of the 2015 NBC.

Both sheds were modelled assuming a constant infiltration rate of 0.109 air changes per hour (ACH). This estimate was based on an assumed rated airtightness of 1.5 ACH @  $\Delta P=50\text{ Pa}$  based on R-2000 benchmark airtightness (NRCan, 2012) and a nominal envelope operating pressure of 4 Pa. The value of 4 Pa is the reference pressure used in ASTM standard E779-19 (ASTM, 2019). No ventilation systems are assumed for either shed.

Only the electrical systems shed was modelled as heated, the diesel generator shed was modelled as passively heated by the diesel generator waste heat. Heating is supplied by two 1.5 kW electric resistance heaters. A two-stage control scheme was modelled using TRNSYS standard library Type 108 (TESS, 2019b). At an interior dry-bulb temperature of  $7.5\text{ }^{\circ}\text{C}$  the first resistance heater is switched on until  $10\text{ }^{\circ}\text{C}$  is achieved. If the interior temperature drops below  $5\text{ }^{\circ}\text{C}$  the second resistance heater is also switched on. The electrical demands for shed heating are added to the other system loads, described in Section 2.3, to be met by the micro-grid.

### 2.2.7 Photovoltaics

The PV generation system was modelled using TRNSYS standard library Type 190 (TESS, 2019b), shown in Figure 2 as “CS6K\_290MS”. Type 190 is a validated empirical steady-state model of PV modules developed by De Soto et al. (2006). This five-parameter model approximates system operating performance by representing PV modules as resistance-diode circuits, illustrated in Figure 7.

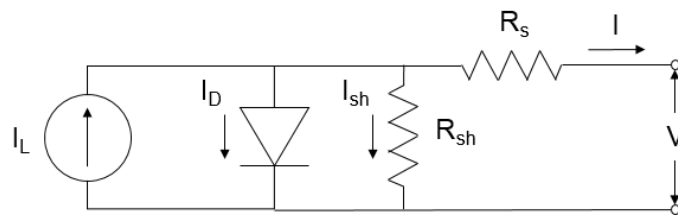


Figure 7. Resistor-diode PV model schematic, adapted from De Soto et al. (2006)

The “five parameters” refers to the circuit element characteristics in Figure 7. These parameters are determined by pre-processing commonly-reported PV manufacturer data using an auxiliary tool that is packaged with distributions of TRNSYS.

For this study, the PV array was assumed to be constructed from individual 290 W PV modules (Canadian Solar, 2018). Type190 model inputs for these modules are described Table 6.

Table 6. Summary of PV module model parameters, based on data from Canadian Solar (2018)

Parameter	Value
Short-circuit current at STC, $I_{SC}$ [A]	9.67
Open-circuit voltage at STC, $V_{OC}$ [V]	39.3
Voltage at maximum power point and STC, $V_{MPP}$ [V]	32.1
Current at maximum power point and STC, $I_{MPP}$ [A]	9.05
Temperature coefficient of $I_{SC}$ at STC [A/K]	0.004835
Temperature coefficient of $V_{OC}$ at STC [V/K]	-0.11397
Number of cells wired in series	60
Extinction coefficient-thickness product of cover	0.013
Module area [m <sup>2</sup> ]	1.457
Five Parameters	
Ideality factor, $a$ [-]	1.576
Light current, $I_L$ [A]	9.682
Diode reverse saturation current, $I_0$ [A]	1.413E-10
Series resistance, $R_s$ [ $\Omega$ ]	0.2735
Shunt resistance, $R_{sh}$ [ $\Omega$ ]	219.2

## System Loads

Based on communication with Polar Knowledge Canada five primary electrical loads were identified:

1. Vehicle block heaters;
2. Facility lights;
3. Facility garage door;
4. Standby loads;
5. Electrical equipment shed heating.

The definitions of the block heaters, lights, garage door, and standby loads are described in the following subsections. The electrical equipment shed heating modelling was described previously in Section 2.2.6.

### 2.3.1 Vehicle Block Heaters

The following assumptions were made for block heating loads:

- The demand of an individual block heater is 650 W;
- It is assumed that three vehicles are plugged in daily from 05h00 to 13h00;
- The plugs are thermostatically controlled such that they only operate when ambient temperatures are at or below -5 °C.

Thermostatic control is modelled using TRNSYS standard library Type 106 (TESS, 2019b). This type models a thermostatic control with setpoint and deadband. For this study the deadband was assumed to be 2 °C.

### 2.3.2 Facility Lights

Based on communication with Polar Knowledge Canada, and the provided electrical plans, 18 lighting fixtures were modelled. Each was assumed to draw 150 W when switched on. The lights are all assumed to have a daily schedule of being on 09h00 to 11h00, and 15h00 to 17h00. This schedule is assumed for every day during the simulation period, including weekends.

### 2.3.3 Facility Garage Door

The micro-grid system is assumed to also power two garage door openers: one primary and one auxiliary. Per the provided electrical plans, each door is assumed to draw 280 W when in operation. Only one door is modelled as operating daily, and it is assumed to have an open-close cycle that occurs three times per day: at 08h00, 12h00, and 16h00. The duration of each opening or closing cycle was estimated assuming a door opening speed of 6 inches/s (Genie, 2017) and a travel distance of 24 feet; therefore, duration is assumed to be 48 seconds. The total open and close cycle is assumed to have a duration of five minutes which is equal to the selected simulation time step.

### 2.3.4 Standby Loads

Standby loads were characterized in the model as a constant baseload due to standby operations of micro-grid and site equipment. From discussions with Polar Knowledge Canada, the following constant loads were assumed:

- 2 emergency light fixtures, each continuously drawing 150 W (one in each shed);
- Constant Inverter standby load of 75 W;
- Constant 240 W representing the collective data acquisition system, battery management system, and sensors standby loads.

Thus, the total constant system baseload is assumed to be 615 W.

## Performance Metrics

Annual performance was characterized using several metrics. The principal metric is annual on-site renewable generation,  $Q_{renew,gen}$  [GJ], which is the total output of wind and solar generation. This metric does not take into account inverter and rectifier losses.

The load cover factor,  $F_{lc}$ , was also used to analyze performance.  $F_{lc}$  is a non-dimensional ratio representing the fraction of annual load that was met by on-site renewable generation. For this study  $F_{lc}$  is expressed as:

$$F_{lc} = \frac{Q_{demand} - Q_{grid} - Q_{diesel \rightarrow load} - Q_{inverter,out} \cdot f_{diesel}}{Q_{demand}} \quad (1)$$

where  $Q_{demand}$  is the annual on-site energy demand [GJ],  $Q_{grid}$  is annual energy import from the grid [GJ],  $Q_{diesel \rightarrow load}$  is the annual electricity supplied directly from the diesel generator to the concurrent site load [GJ], and  $Q_{inverter,out}$  is the annual energy supplied from the inverter to the on-site demand [GJ]. A value of 1 indicates all loads were covered by the renewable system, and a value of zero indicates that no energy supplied by renewable generation.

$Q_{inverter,out}$  is multiplied by factor  $f_{diesel}$  in Equation 1 to account for the fact that some of the energy supplied from the battery originated from excess diesel generation:

$$f_{diesel} = \frac{Q_{diesel \rightarrow rect}}{Q_{PV \rightarrow load} + Q_{PV \rightarrow battery} + Q_{wind \rightarrow rect} + Q_{diesel \rightarrow rect} - Q_{rect,loss} - Q_{battery,loss} - Q_{inv,loss}} \quad (2)$$

where  $Q_{diesel \rightarrow rect}$  is the annual energy transferred from the diesel generator to the rectifier [GJ],  $Q_{wind \rightarrow rect}$  is the annual energy transferred from the wind turbine to the rectifier [GJ],  $Q_{PV \rightarrow load}$  [GJ] is the total annual PV generation sent directly to the inverter to meet concurrent AC site demands,  $Q_{PV \rightarrow battery}$  [GJ] is the annual PV

generation charged directly to the battery,  $Q_{rect,loss}$  [GJ] is the annual rectifier losses,  $Q_{battery,loss}$  [GJ] is the annual battery system losses, and  $Q_{inv,loss}$  [GJ] is the annual inverter system losses.

Also reported with the simulation results is the amount of annual renewable generation that is dumped,  $Q_{renew,dump}$  [GJ]. Mentioned previously in Section 2.2.5, renewable generation is sent to a dump load when the battery is fully-charged and there is no concurrent load to consume the generation. A non-zero value of  $Q_{renew,dump}$  may be indicative of over-sized renewable generation capacity and/or under-sized on-site energy storage.

$Q_{renew,dump}$  is also used to calculate the annual renewable generation utilization factor,  $F_{util}$ :

$$F_{util} = \frac{Q_{renew,gen} - Q_{renew,dump}}{Q_{renew,gen}} \quad (3)$$

which is a ratio of renewable generation consumed or useable by the system, to total generation. Like,  $F_{lc}$ ,  $F_{util}$  varies between zero and one, where one indicates all renewable generation can be used by the system and a value of zero indicates no renewable generation is useable by the system.

Finally, system performance is evaluated in terms of annual carbon dioxide equivalent ( $CO_{2e}$ ) emissions reductions. To determine the annual emissions savings, baseline annual  $CO_{2e}$  emissions were determined assuming all the loads are met with grid connected electricity. In Qulliq Energy Corporation's (QEC's) 2018/19 general rate application document (QEC, 2017), a weighted average diesel fuel efficiency rate of 3.70 kWh<sub>e</sub>/litre was reported for Cambridge Bay. ECCC (ECCC, 2021b) reports that combustion of diesel produces 2681 grams of  $CO_2$  per litre, 0.078 grams of  $CH_4$  per litre, and 0.022 grams of  $N_2O$  per litre. In this analysis these emissions species were represented as a single combined carbon dioxide equivalent emission,  $CO_{2e}$ , per litre of diesel.  $CO_{2e}$  represents the quantity of  $CO_2$  which has the same global warming potential as a given mixture of combustion products. The  $CO_{2e}$  of  $CH_4$  and  $N_2O$  were determined using the EPA (2019)  $CO_{2e}$  calculator, and the emissions factors, expressed in both grams of molecule per litre of fuel and grams of  $CO_{2e}$  per litre of fuel are summarized in Table 7.

Table 7. Summary of emission factors from diesel combustion

Gas	Emission Factor [g/litre]	Emission Factor [g $CO_{2e}$ /litre]
$CO_2$	2681	2681
$CH_4$	0.078	2.000
$N_2O$	0.022	6.600

Summing the  $CO_{2e}$  per litre values in Table 7, the emissions factor for diesel combustion is estimated to be 2690 grams  $CO_{2e}$  per litre. Using the reported fuel conversion efficiency (kWh<sub>e</sub>/litre) from QEC, the emission factor may be recast as 727 grams  $CO_{2e}$  per kWh of electricity produced. It is assumed that the fuel efficiency reported by QEC (2017) is the ratio of total plant fuel consumption divided by total generation, and does not account for system losses such as transmission, distribution, and station service loads. In the rate application document, it is reported that for Cambridge Bay, 5.7% of total generation is attributed to losses and station service loads. Therefore, the fuel efficiency of the grid was reduced to 3.49 kWh<sub>e</sub> of electricity delivered to the building site per litre of diesel fuel consumed, and the grid emission factor was readjusted to 768  $CO_{2e}$  g/kWh<sub>e</sub> to account for transmission and distribution losses.

### 3 Simulation Cases

An initial simulation was conducted to establish base energy performance of the proposed renewable generation. This system used the loads described in Section 2.3, and the micro-grid systems as described in Sections 2.2.2 to 2.2.6. The only renewable generation system in the base system is the single SD6 wind turbine, and the 22.8 kWh battery system; PV is not included in the base system. Once base system performance was established the following scenarios were examined:

1. Variation of site battery capacity;
2. Integration of solar PV;
3. Sensitivity to site electrical demands.

#### Battery Size Variation

The function of the battery storage is to address temporal mismatches of on-site renewable generation and site demands. The purpose of this simulation was to analyze how doubling the capacity of the batteries in the system impacts performance relative to the base system. This was accomplished in the model by increasing the number of parallel batteries from 6 to 12, and doubling the maximum power draw of the batteries permitted by the grid controller.

#### 3.2 Integration of Solar PV

Shown previously in Figure 5, the grid controller algorithm implemented in TRNSYS was designed to accommodate the inclusion of solar PV generation connected to the micro-grid. This simulation analysis was divided into two steps: the first was to perform a parametric study of annual performance of a single PV module located in Cambridge Bay, Nunavut. The module azimuth,  $\gamma$ , and slope,  $\beta$ , were varied from facing due east, through south, to due west, and from horizontal to vertical; these orientation angles are illustrated in Figure 8. The objective of this simulation was to determine the optimal orientation for site solar PV production, and to evaluate how the annual solar production curve changes with orientation.

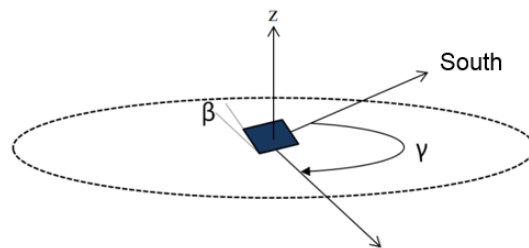


Figure 8. PV panel azimuth and slope angle definitions

Output of this parametric study, and review of the site electrical demand profile, were then used to size and orient a PV array which was then added to the base system model. Performance of the PV-integrated system was simulated and compared to base system performance.

#### Load Sensitivity

The system demands described in Section 2.3 are best estimates based on discussions with Polar Knowledge Canada. Since there is high uncertainty in these estimates, a sensitivity study was undertaken which varied the load estimates and evaluated the impacts to system performance. Two additional demand scenarios were developed and used.

Demand Scenario B examined the impact of extreme loading from block heaters. Stated in Section 2.3.1 it is assumed that three receptacles are used for block heating. The electrical plans provided from Polar Knowledge Canada lists up to twelve receptacles of block heating on the panel. Therefore, as a “high demand” scenario the block heater loads were increased in Demand Scenario B to simulate all twelve receptacles in use. The schedule and thermostatic control described previously in Section 2.3.1 was still used. Demand Scenarios C also assumed all twelve receptacles are in use, but the duration of the load was reduced by 50%. This was accomplished by having the block heaters only operational from 05h00 to 09h00.

## 4 Results

### Baseloads

Figure 9 plots the daily electrical demand profile for the base system scenario, excluding space heating demands. For the duration of the profile plotted in Figure 9, the ambient temperatures were below -5 °C, thus block heating receptacles were on during the entire scheduled operation period.

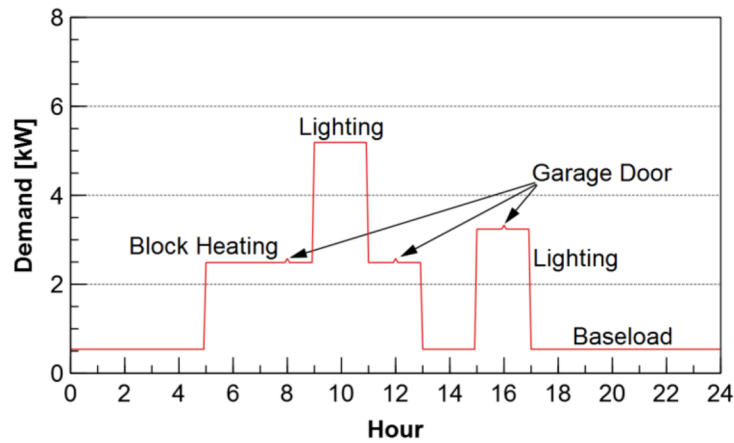


Figure 9. Daily electrical demand profile, excluding space heating

The total daily electrical demand in Figure 9 is 39.4 kWh<sub>e</sub>. The electrical demand profile for shed spacing heating varied based on ambient conditions and internal gains from the micro-grid systems. Figure 10 plots the electrical demand for shed spacing heating during the first week of January.

Figure 10. Simulated space heating electrical demand for first week of January

It can be seen in Figure 10 that for this entire period only the first stage of heating was used since demand never exceeded the 1.5 kW of a single electric resistance heater.

Figure 11 plots the load-duration curve of the site demands. This graph provides information on the cumulative hours per year the site electric power demands are at a certain magnitude or greater. For example, at 2800 hours the value on the curve is 2.0 kW. Thus, for 2800 hours of the year the site demand is 2.0 kW or greater. Curves

like the one Figure 11 are useful for system capacity planning; they identify peak and baseload demand and help size primary, and auxiliary peak generation, systems. The peak demand in Figure 11 is 6.7 kW and has a cumulative duration of 72 hours.

Figure 11. Site demands load-duration curve

Annual on-site energy demand of the base system is 50.2 GJ (13.9 MWh). By end-use, the annual demands are:

- Block heating: 12.6 GJ (3.5 MWh);
- Lighting: 14.2 GJ (3.9 MWh);
- Space heating: 3.9 GJ (1.1 MWh);
- Emergency Lighting: 9.5 GJ (2.6 MWh);
- Data acquisition system and sensors: 7.6 GJ (2.1 MWh);
- Inverter standby system: 2.4 GJ (0.7 MWh).

## Base Case System Performance

The annual flow of energy through the base system is summarized in the Sankey diagram in Figure 12.

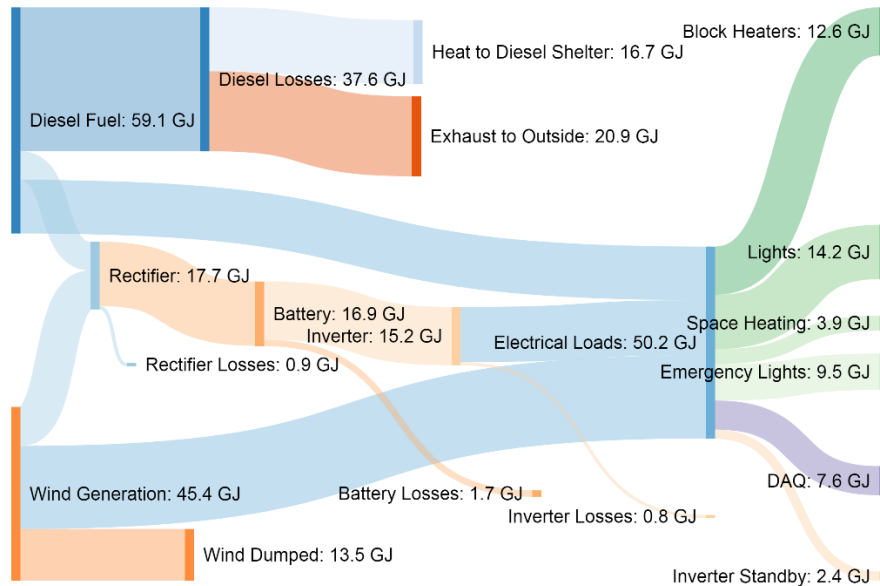


Figure 12. Base renewable system annual energy flow

The annual load for garage door operation was calculated to be 29.4 MJ, or 0.0294 GJ, and is therefore omitted from Figure 12 for clarity.

The system was able to meet all loads using the on-site renewable generation system and diesel back-up system; thus there was no import required from the external grid. The annual production of the 6 kW wind turbine is estimated to be 45.4 GJ (12.6 MWh). Of that total output, 13.5 GJ, or 30%, was directed to a dump load which equates to a utilization factor,  $F_{util}$ , of 70%. The load cover factor,  $F_{lc}$ , is 56%; i.e., 56% of the on-site electrical demands were met by the renewable generation system.

The on-site diesel generation system is estimated to consume 59.1 GJ of fuel per year. The diesel generator model Type 120 in TRNSYS intrinsically assumes a lower heating value of 35.5 MJ per litre. Thus, annual fuel consumption may be expressed as 1665 litres per year. Using the 2690 grams  $CO_{2e}$  per litre emission factor for diesel fuel combustion derived previously in Section 2.4, the emissions from diesel generator operation in the base system is estimated to be 4.5 tonnes  $CO_{2e}$ /year.

Annual  $CO_{2e}$  savings realized by the base system was calculated by comparing the annual base system emissions to annual emissions that would have been produced if all site demands were met by the external utility. When calculating emissions of the no-renewables scenario it was assumed there were no demands from inverter standby, data acquisition system, space heating, or emergency lights since these are all components of the renewable generation system itself and would not be present if no on-site renewables were installed. Thus, the reference annual demand is the sum of block heating and lighting demands which is equal to 26.8 GJ (7.4 MWh). Using the electrical grid emission factor derived previously in Section 2.4, this annual demand being met by the grid equates to annual emissions of 5.7 tonnes  $CO_{2e}$ /year. With 5.7 tonnes  $CO_{2e}$ /year as the no-renewables reference, the base renewable system is estimated to reduce annual emissions by 21%.

The annual performance metrics of the base case renewable generation system is summarized in Table 8.

Table 8. Summary of base system system annual performance metrics

Performance Metric	Value
Total site demand, $Q_{demand}$ [GJ]	50.2
Total annual wind production, $Q_{wind,gen}$ [GJ]	45.4
Annual utilization factor, $F_{util}$ [%]	70%
Annual load cover, $F_{lc}$ [%]	56%
Annual CO <sub>2e</sub> emission reduction [%]*	21%

\*Relative to emissions if all loads met by grid

Figure 13 plots the monthly energy balance of the base case system.

Figure 13. Base system monthly energy balance

For each month, the stacked columns on the left are the sum of energy input into the system, and the stacked columns on the right are the sum of energy outputs and end-uses. For each month there was no diesel generation dumped or extra electrical consumption from the utility grid. The seasonal variation in electrical loads is driven solely by the seasonal variation in block and space heating demands. Differences between adjacent bars in a given month varied from 0.3 to 17 kWh throughout the year which occurred due to system battery storage carrying energy over to the next month.

Finally, Figure 14 replots the Figure 11 site load-duration curve with the generation-duration curves of the wind and diesel generation system. Also plotted is the SOC duration curve for the battery system.

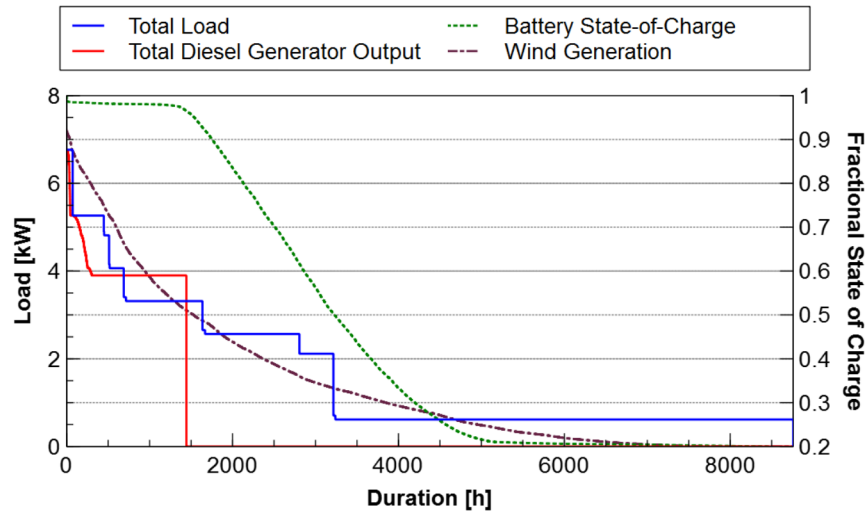


Figure 14. Base system load, generation, and battery state-of-charge duration curves

The load-duration and wind generation duration curves in Figure 14 both follow a similar trend. At first glance this suggests capacity of the wind generation system is suited to site demands. Reconsidering the Sankey diagram in Figure 12, however, it is shown that there is still a need for supplementary diesel generation, and periods where wind generation must be dumped. This dumping of wind generation occurs because there are temporal mismatches between wind generation and renewable demand. The battery system is used to bridge this gap, but during periods of surplus generation where the battery is fully charged the surplus must be dumped or generation curtailed.

Figure 14 also shows that for the majority of its operating time during the year the diesel generator is operating at its minimum output. Figure 12 shows, however, that all surplus diesel generation when operating at the minimum point was able to be stored in the battery system, and did not require use of the dump load. The average annual fuel efficiency of the on-site diesel generator was estimated to be 3.60 kWh<sub>e</sub> per litre which is higher than the assumed grid efficiency of 3.49 kWh<sub>e</sub> per litre.

Finally, the battery SOC duration curve on Figure 14 indicates that the battery has a state-of-charge greater than or equal to 97% for approximately 1400 hours (16 % of the year), and is at the minimum SOC for approximately 3760 hours (42% of the year).

## Battery Capacity Study

To better utilize surplus on-site renewable generation during periods of low site demand, the battery capacity of the system was simulated as being doubled from 22.8 kWh to 45.6 kWh. The resulting annual energy flow of this system is summarized in the Sankey diagram of Figure 15.

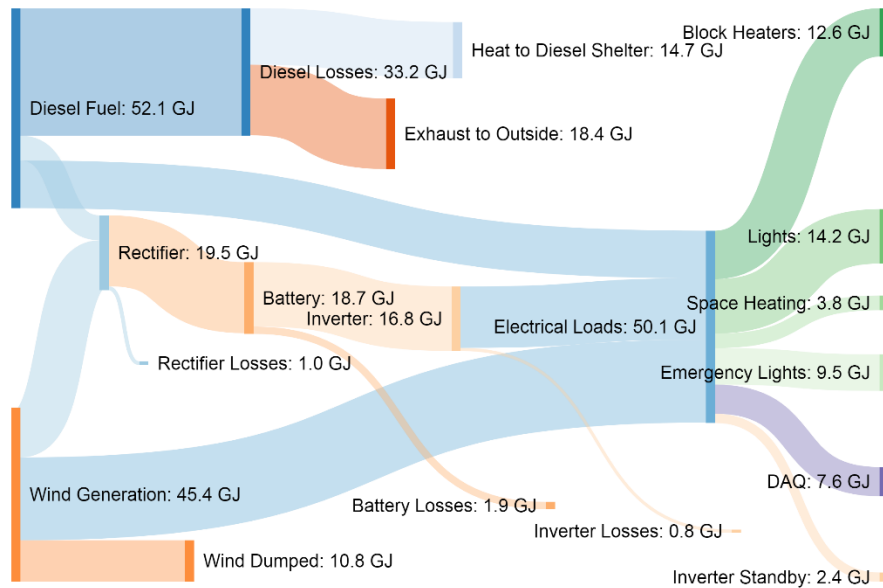


Figure 15. Double battery capacity system annual energy flow

As expected, total annual wind generation is identical to the base system in Figure 12, since this value only varies with climate conditions, which are identical for both simulations. Additionally, the block heating, lighting, emergency lights, and data acquisition loads are also all identical to the base system. These loads are either prescribed scheduled loads that are the same for both scenarios, or in the case of the block heaters a function of ambient temperatures which again are identical for both simulations. The space heating load, however, is shown to change. This is due to changes in internal gains of the shed equipment from the battery system. The base case had an annual battery system loss of 1.7 GJ per year which were passed as internal gains to the equipment shed enclosure, and thus offset heating demand. For the increased battery capacity scenario the annual battery system loss is shown in Figure 15 to increase to 1.9 GJ per year.

Comparing Figure 15 to Figure 12 it can also be seen that both diesel fuel consumption and wind generation dumped decreased due to increased battery capacity. Table 9 summarizes the annual performance metrics for the system with double battery capacity, and compares them to the base system performance metrics presented previously in Table 8.

Table 9. Comparison of double battery capacity and base system annual performance metrics

Performance Metric	Double Battery Capacity	Base System
Annual utilization factor, $F_{util}$ [%]	76%	70%
Annual load cover, $F_{lc}$ [%]	63%	56%
Annual CO <sub>2e</sub> emission reduction [%]*	31%	21%

\*Relative to emissions if all loads met by grid

Doubling the capacity of the battery is shown here to improve all annual performance metrics by a material amount relative to the base case.

## Solar PV Study

### 4.4.1 Site Solar Resource Study

Prior to integrating a PV system into the base system model, a parametric study was conducted to evaluate the variation of annual production of a single PV module as a function of module orientation. The results of this parametric study is summarized in Figure 16.

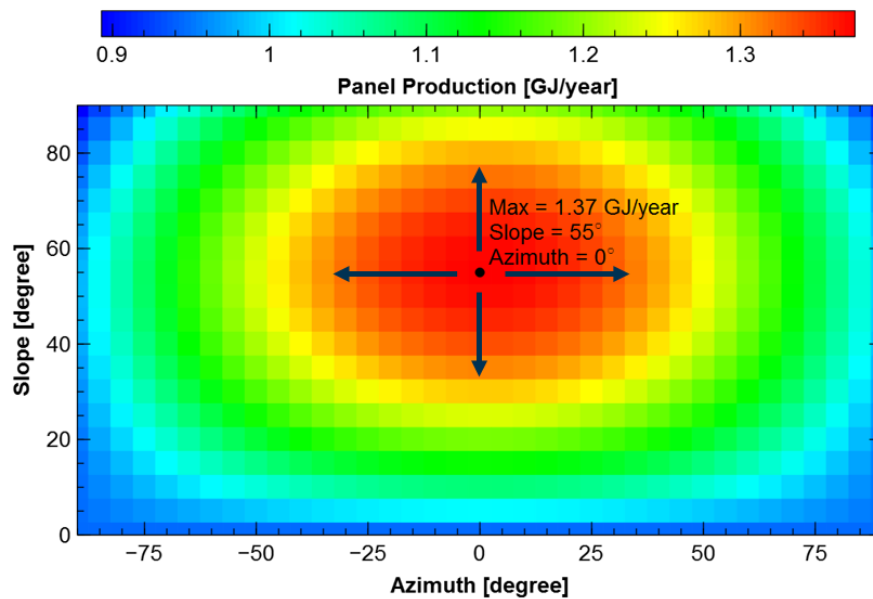


Figure 16. Annual PV module production parametric study

A slope of  $\beta = 55^\circ$  and azimuth of  $\gamma = 0^\circ$  is shown to yield a maximum annual production of 1.37 GJ/year/module. It was also found that near this optimal point annual production is relatively insensitive to orientation. For example, varying the slope by  $\pm 20^\circ$  yielded annual production reductions of up to 4%. Varying the azimuth by  $\pm 35^\circ$  reduced annual production by up to 5%.

Figure 17 plots the monthly production of the PV module when in the optimal orientation for annual energy production.

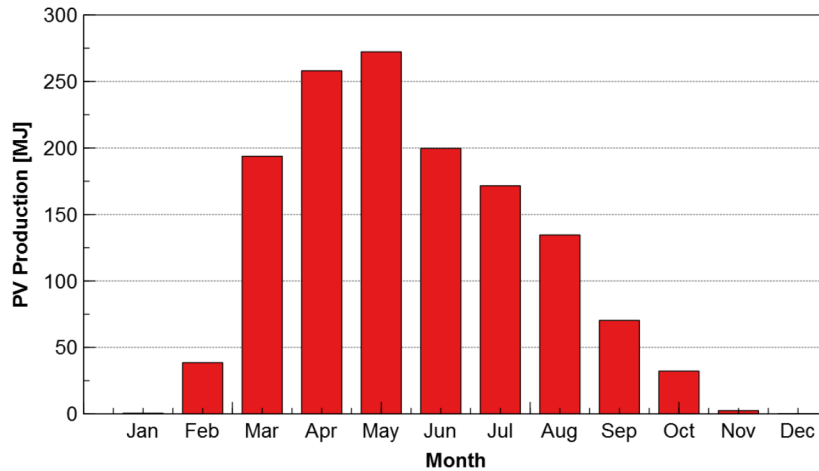


Figure 17. Monthly PV module production at optimal point

Production is shown to peak in the month of May, then reduces to zero production in the month of December.

The monthly production profile of Figure 17 can be manipulated by varying the module slope. For example, Figure 18 compares the monthly profile of Figure 17 ( $\beta = 55^\circ$ ) to monthly production profiles of modules that have had module slope increased and decreased by  $20^\circ$ .

Figure 18. Variation of PV seasonal production curve and slope

Figure 16 had previously shown that by varying  $\beta$  by  $\pm 20^\circ$  annual production decreased by up to 4%. Figure 18 shows that varying slope also shifts the monthly production profile. By increasing the slope to  $\beta = 75^\circ$  (more vertical), there is more production in the month of February and March compared to the optimal orientation. By decreasing the slope to  $\beta = 35^\circ$  (more horizontal), production in June and July increases relative to the optimal orientation.

Altering module azimuth,  $\gamma$ , affects the daily production profile. For example, Figure 19 plots the July average daily production curves of PV modules with azimuth angles of  $-35^\circ$ ,  $0^\circ$ , and  $35^\circ$ .

Figure 19. Variation of PV daily production curve and azimuth for month of July

The  $\gamma = 0^\circ$  curve represents the PV module average production profile when it is oriented in the optimal position ( $\beta = 55^\circ$ ). If the module azimuth is turned  $35^\circ$  due east ( $\gamma = -35^\circ$ ) while keeping module slope fixed at  $55^\circ$ , production is higher in the morning and peaks earlier. If the module is instead turned  $35^\circ$  due west ( $\gamma = 35^\circ$ ) production is higher in the afternoon and peaks later in the day.

Such considerations of how orientation affects the monthly and daily generation profile is important when designing the PV system since this information allows designers to not only maximize annual production, but also better match generation with site-demands. As can be seen in Figures 12 and 15 when surplus renewable generation is passed to the battery systems energy losses are incurred from battery charge and discharge. Thus it is desirable to match generation with concurrent demand as much as possible, but also balance the production losses associated with orienting the PV array off annual-optimal against savings potential savings from better matching generation and demand.

#### 4.4.2 PV Integration into System

Analyzing both the monthly site demands in Figure 13 and the PV module production profile in Figure 17 it was decided to size the system such that it will produce 2000 MJ in the month of May to offset the diesel generation for that month. May was selected since it's was found to be the peak production month of the PV module when oriented for maximum annual production. Using Figure 17, a single PV module at  $\beta = 55^\circ$  and  $\gamma = 0^\circ$  is estimated to have a May production of 270 MJ. Therefore, an integrated array of 8 modules was added to the base system which equates to an array power rating of 2.32 kW. Figure 20 illustrates the Sankey diagram of the system annual energy flow of this system.

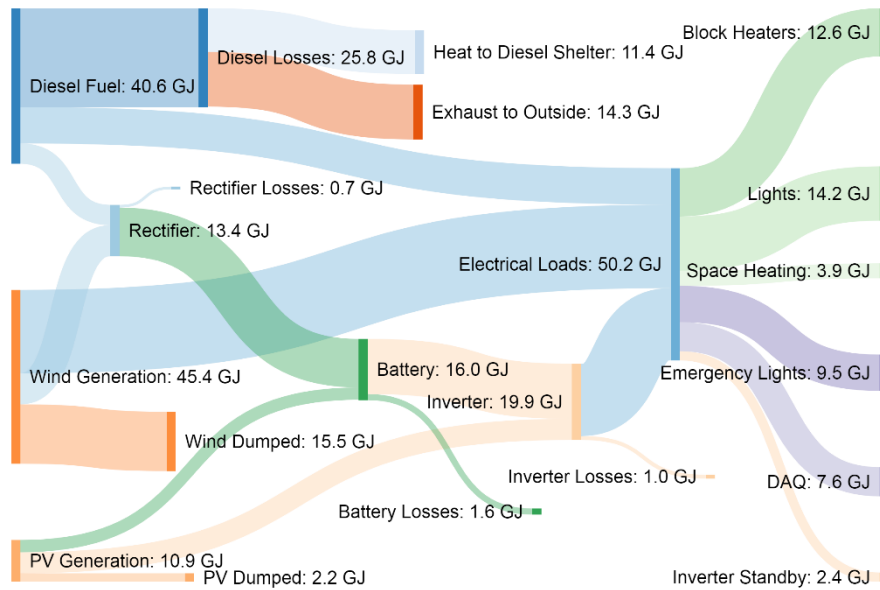


Figure 20. Annual energy flow of base system with integrated PV

In Section 4.1 it was estimated that if the system loads were all met with grid-supplied electricity annual emissions would equate to 5.7 tonnes of CO<sub>2e</sub>/year. The base case renewable system (wind, battery, and no PV in Section 4.2) was estimated to generate 4.5 tonnes of CO<sub>2e</sub>/year; a reduction of 1.2 tonnes or 21%. The addition of the 2.32 kW PV array to the base case renewable system considered here is estimated to have annual system emissions of 3.1 tonnes of CO<sub>2e</sub>/year; i.e. an additional 1.5 tonnes of CO<sub>2e</sub>/year reduction compared to the base case renewable system, and a reduction of 46% relative to meeting the site loads with grid electricity. Table 10 provides a summary and comparison of the annual performance metrics of the PV integrated system to the base case system.

Table 10. Comparison of integrated PV and base system annual performance metrics

Performance Metric	Integrated PV	Base System
Annual utilization factor of wind, $F_{util}$ [%]	66%	70%
Annual utilization factor of PV, $F_{util}$ [%]	80%	N/A
<b>Annual utilization factor of all renewable, <math>F_{util}</math> [%]</b>	<b>69%</b>	<b>70%</b>
Annual load cover, $F_{lc}$ [%]	71%	56%
Annual CO <sub>2e</sub> emission reduction [%]*	46%	21%

\*Relative to emissions if all loads met by grid

Both annual load cover and emissions reduction are shown to improve relative to the base system. Utilization of the wind generation is shown, however, in Table 10 to decrease. This is due to the grid controller giving priority to charging the battery with excess DC renewable generation first over excess AC current generation. This control decision was made since DC generation can be supplied directly to the battery whereas AC generation must be passed through the rectifier.

Figure 21 plots the monthly energy balance of the micro-grid system with integrated PV.

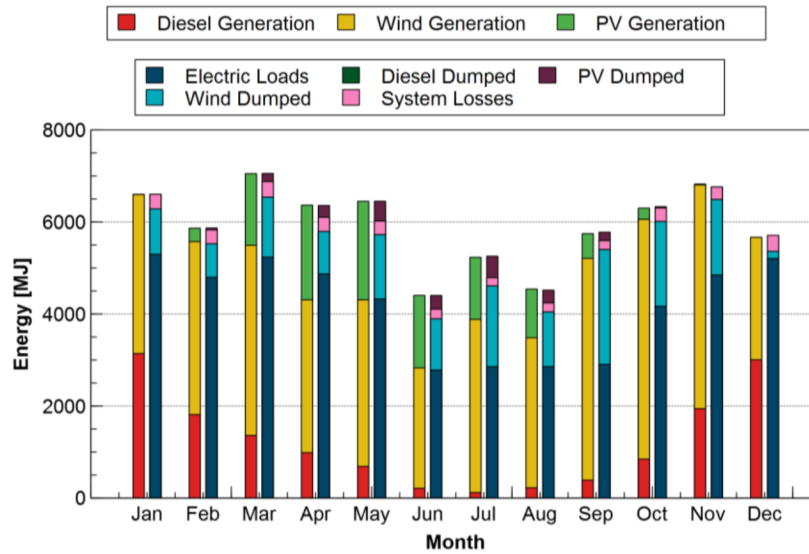


Figure 21. System with integrated PV monthly energy balance

Compared to the monthly balance of the base system, plotted in Figure 13, there is significant reduction in diesel generation for the months of March to July. A numerical comparison of the monthly diesel generation of the system with and without integrated PV is provided in Table 11.

Table 11. Comparison of base and integrated PV systems monthly diesel generation

Month	Diesel Generation [GJ]		% Reduction
	Base System	Integrated PV	
Jan	3.1	3.1	0%
Feb	2.0	1.8	10%
Mar	2.6	1.4	46%
Apr	2.6	1.0	62%
May	2.1	0.7	67%
Jun	1.2	0.2	83%
Jul	0.6	0.1	83%
Aug	0.7	0.2	71%
Sep	0.6	0.4	33%
Oct	1.0	0.8	20%
Nov	2.0	1.9	5%
Dec	3.0	3.0	0%

## Baseload Sensitivity Study

The final study of this report examined the sensitivity of base system (no PV, wind turbine, and 22.8 kWh battery storage) to variations in baseload assumptions. Two alternate load scenarios were considered, described previously in Section 3.3.

### 4.5.1 Scenario B: Quadrupled Block Heater Loads

Figure 22 plots the annual energy flow for the base system with the number of active block heater receptacles increased from three to twelve (Scenario B).

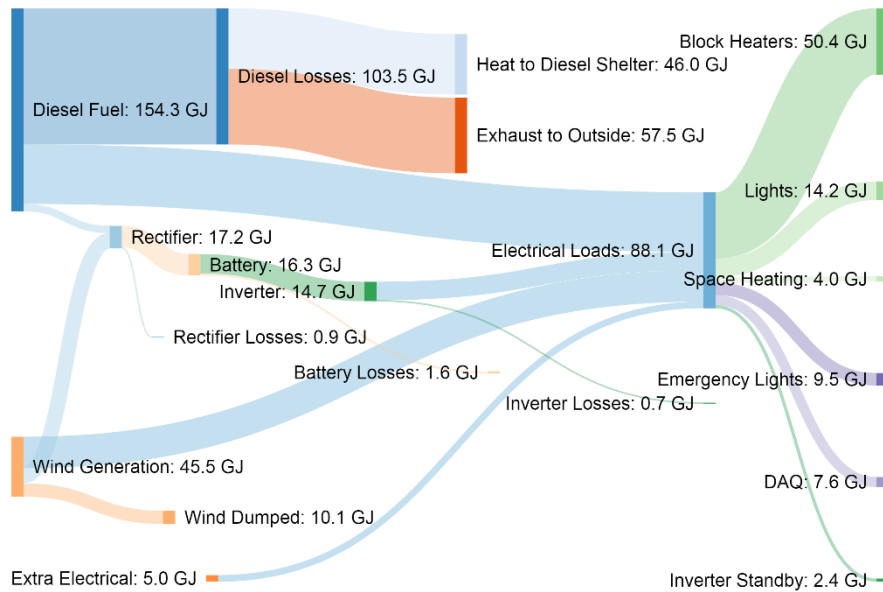


Figure 22. Load scenario B annual system energy flow

It can be seen that the block heating energy use in Figure 22 has quadrupled compared to the base system energy use, shown in Figure 12. All other energy end-use quantities are found to be similar to the base system. Total wind generation also does not change, but annual diesel fuel consumption increases from 59.1 GJ to 154.3 GJ to meet the site increased loads. More wind generation is utilized relative to the base system, with 10.1 GJ dumped annually instead of 13.5 GJ. Unlike the base system, there is also a need for an additional 5.0 GJ per year from an external grid source to meet these loads. The annual performance metrics are summarized and compared to the base case demand in Table 12.

Table 12. Impact of increased block heating loads (Scenario B) on base system performance

Performance Metric	Scenario B	Base Case Demand
Annual utilization factor of wind, $F_{util}$ [%]	78%	70%
Annual load cover, $F_{lc}$ [%]	43%	56%
Annual CO <sub>2e</sub> emission reduction [%]	7%	21%

To calculate the annual CO<sub>2e</sub> emission reduction for the increased block heating demand Scenario B, the baseline emissions with no renewable generation needed to be recalculated to account for the increased annual site demands. Using the same approach described in Section 4.2, the no-renewables annual site demand was calculated to be 64.6 GJ (17.9 MWh<sub>e</sub>) per year which equates to 13.8 t CO<sub>2e</sub> per year from grid-related emissions. The 154.3 GJ per year of diesel fuel consumption shown in Figure 22 equates to 11.7 t CO<sub>2e</sub> per year, and the additional 5.0 GJ per year from the grid contributes an additional 1.1 t CO<sub>2e</sub> per year yielding total system emissions of 12.8 t CO<sub>2e</sub> per year, and annual emissions savings of 7% compared to if no renewable generation was used to meet Scenario B loads.

### 4.5.2 Scenario C: Doubled Block Heater Loads

Figure 23 plots the annual energy flow of the base system when demand Scenario C is assumed. This scenario models all twelve block heating receptacles in use, but only from 05h00 to 09h00.

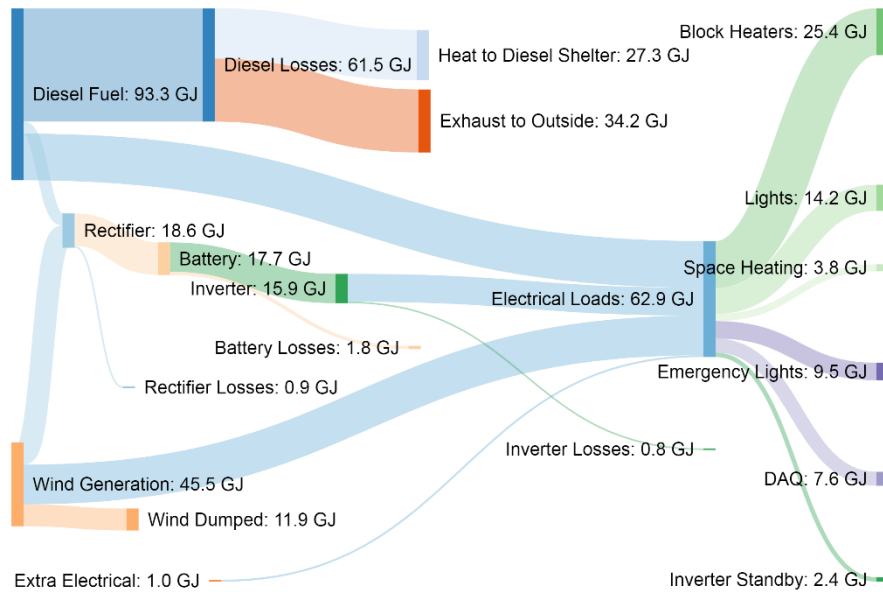


Figure 23. Load scenario C annual system energy flow

The annual block heating demand in Figure 23 is 25.4 GJ per year; half the total energy demand of Scenario B but twice the annual demand of the base case load scenario. The annual performance metrics are summarized and compared to the base case demand in Table 13.

Table 13. Impact of increased block heating loads (Scenario C) on base system performance

Performance Metric	Scenario C	Base Case Demand
Annual utilization factor of wind, $F_{util}$ [%]	74%	70%
Annual load cover, $F_{lc}$ [%]	50%	56%
Annual CO <sub>2e</sub> emission reduction [%]	13%	21%

Like Scenario B, the no-renewables reference annual emissions needed to be recalculated. The annual sum of block heating and lighting energy consumption is 39.6 GJ (11.0 MWh<sub>e</sub>) which equates to annual emissions of 8.4 t CO<sub>2e</sub> per year if the load is met solely by the local utility grid. From the data in Figure 23, 93.3 GJ of diesel fuel is consumed, which equates to 7.1 t CO<sub>2e</sub> per year. Additionally, 1.0 GJ of auxiliary grid energy is required which equates to 0.2 t CO<sub>2e</sub> per year. Thus, total emissions for the system in Figure 23 is estimated to be 7.3 tonnes CO<sub>2e</sub> per year, with relative annual emissions savings of 13%.

## 5 Discussion

The base micro-grid system is estimated reduce annual CO<sub>2e</sub> emissions by 21% when base case site energy demands are assumed, and 56% of the site demands are met by on-site renewable generation. In Figure 12, it was shown that the 6 kW wind turbine is estimated to produce 45.4 GJ per year of renewable generation. Comparing that the estimated 50.2 GJ per year in site demands, it can be seen that under current load consumptions the base system cannot cover all site demands.

It is additionally shown in the results that 30% of the annual wind generation could not be utilized, and was therefore directed to a dump load. The reason for this is both temporal mismatch of on-site generation and demand, and limited on-site storage capacity. Figure 9 previously illustrated that base case peak site demands occur around 10h00 and 16h00. Daily wind generation, however, is distributed through the day. This is illustrated using the average daily wind generation profile plotted in Figure 24.

Figure 24. Average daily wind generation profile

To bridge the gap between electricity generation and demand, a 22.8 kWh<sub>e</sub> battery storage system is used in the micro-grid considered in this study. It was shown in Section 4.3 how doubling the battery capacity of the system can improve annual system performance by enabling more storage of on-site generation and subsequent reduction in energy directed to the dump load. For this micro-grid system, doubling the battery capacity increases wind generation utility,  $F_{util}$ , from 70% to 76%, and annual emissions reductions increase from 21% to 31%. It should be noted, however, that a previous study on PV and battery storage system sizing in Cambridge Bay, Nunavut, from Wills et al. (2019) demonstrated that as storage capacity is increased there is a diminishing return in system performance gains.

While the base system analyzed here focused on on-site wind generation, inclusion of a PV array was also considered. Given the high latitude of Cambridge Bay, there is significant variation in seasonal solar generation, as illustrated in Figure 17. Additionally, comparing the monthly site demands in Figure 13 to the monthly PV generation in Figure 17, it can be seen that there is a significant seasonal mismatch between site demand and PV generation, with peak PV generation occurring in May and peak demand in January. The PV array modelled in this study was sized and oriented such that PV production during the peak production month equalled the total diesel energy consumption estimated for that month in the base case system which uses wind generation only. The results in Section 4.4.2 show that using this system and sizing approach annual site diesel consumption is reduced by 67%, and annual emissions savings increase from 21% to 46% relative to the base system, with 71% of site demands being met by renewable energy compared to 56% in the wind only base system. These findings illustrate that although there is a significant seasonal variation of PV generation, and a significant generation-demand temporal mismatch, integrating a PV system into the base system may provide considerable emissions reductions and greater coverage of site demands by on-site renewables.

The optimal orientation in Cambridge Bay for annual solar production is estimated to be at a slope of 55° facing due south; this was the orientation used for the PV integration simulations described in the previous paragraph. The PV orientation analysis in Section 4.4.1 also demonstrated that the shape of the daily and monthly production curve can be changed by altering array azimuth and slope angles respectively. Varying array azimuth by ± 35° is shown to move peak daily production between 11h00 and 15h00 while reducing annual production by 5%. Similarly varying array slope by ± 20° can shift PV production to earlier or later in the year while only decreasing annual production by up to 4%. How the PV production curve can be altered to better match site demands is an important system design consideration, since better matching of load and generation reduces system losses associated with energy storage. However, the savings realized by better demand-generation matching needs to be balanced against losses in annual system production.

The final analysis in this study assessed the sensitivity of system performance to site demands using two additional demand scenarios. The extreme scenario, referred to as Scenario B, assumed that all twelve block heater receptacles planned for the site are in use from 05h00 to 13h00, resulting in a quadrupling of the base case block heater annual energy demand. Scenario C also assumed twelve receptacles in use, but only half the duration per day (05h00 to 09h00) resulting in a doubling of annual block heater energy consumption relative to the base case demands. Both scenarios were found to increase  $F_{util}$  to 78% and 74%, respectively, compared to the base system performance of 70%. However, the annual emissions savings decreased relative to the base demand case due to increased reliance on-site diesel generation and auxiliary energy supply by the grid to meet the loads. The base system and site demands is estimated to yield annual emissions savings of 21% compared to supplying all site demands with grid energy, whereas Scenarios B and C are estimated to achieve 7% and 13% savings, respectively. Increased battery capacity would improve  $F_{util}$  and emissions savings as it would enable more on-site renewable generation to be stored and used to meet site demands.

As a final note, the renewable generation performance estimates provided in this report should be considered as ideal. The system model does not account for reduced performance of the wind turbine due to icing on the blades or other performance degradation factors, nor does it account for turbine down time for maintenance or repairs. Similarly, the solar PV model does not account for snow cover on the array or any other causes of decreased output. While the model makes adjustments to calculated ground reflected radiation to account for snow accumulation, the array itself is always assumed to be clear of snow and dust.

## 6 Conclusions

Using the assumed base case base site demands, the renewable micro-grid system proposed for CHARS is estimated to achieve 21% in annual CO<sub>2e</sub> emissions compared a scenario where those demands are met by the local utility electrical grid. The 6 kW SD6 wind turbine is estimated to produce 45.4 GJ of electrical energy per year. With the given site demands and 22.8 kWh<sub>e</sub> on-site battery capacity, it is estimated that 70% of this annual wind generation can be utilized by the system. Since it is assumed that net-metering of the wind generation is not possible due to infrastructure constraints, the remaining 30% of the potential wind generation must be curtailed or directed to dump loads.

Doubling the 22.8 kWh<sub>e</sub> battery capacity was shown to increase both annual utilized wind generation and emissions reductions by 76% and 31%, respectively. Given that site demands have a relatively high temporal variation whereas wind generation is more uniformly distributed, use of on-site energy storage is crucial to bridging the gap between renewable generation and demands. Previous studies have shown that increasing battery capacity alone for renewable system yields diminishing returns, and therefore further analysis would be needed to determine the optimal battery capacity in terms of technical and economic performance indicators.

Solar was also considered in this study as a renewable generation technology at the CHARS site. The solar resource analysis conducted here highlighted that given the high latitude of Cambridge Bay there is significant variation in solar production compared to southern locations, with peak production occurring in May, and

negligible production in December and January. Additionally, the site demands are seasonally mismatched with solar production, with a demand peak in the winter months and minimal demand the summer. Nonetheless, the simulation of including a 2.32 kW PV array connected to the proposed micro-grid is estimated to increase annual emissions savings to 46%, with 71% of the site demands covered by renewable energy. This was accomplished by the solar PV system significantly reducing and offsetting diesel generation during the late spring and summer months. Thus, despite the high seasonal variability and generation-demands mismatch, solar is shown here to significantly improve emissions savings and load cover that can be provided by the system.

It was noted that the site demand estimates contain a significant amount of uncertainty. Two additional demand scenarios were considered that reflected extreme demand scenarios: doubling and quadrupling the block heating annual demands. The results demonstrated that while more on-site wind generation may be utilized rather than dumped, the relative annual emissions savings of the system decreased significantly. This highlights the sensitivity of system annual performance to the assumed loads.

Based on the load profiles estimated for the application of this renewable energy system, block heating and lighting are the predominant loads. Maximizing the proportion of demand met by renewable sources and minimizing CO<sub>2</sub>e emissions can be achieved with thoughtful specification of equipment and management of site energy demands. For the block heating loads, activation was assumed for temperatures of -5°C or lower, whereas this temperature set point could be reduced to -10°C or -20°C. For the lighting loads, the efficiency of LED lighting, the design lighting power density, and the operation of the lights should be carefully considered to minimize the load while still providing sufficient lighting quality. Finally, minimizing the constant loads of the emergency lighting and DAQ are also aspects of performance optimization to consider.

## 7 Acknowledgements

The authors would like to acknowledge Polar Knowledge Canada for their funding towards this project, and collaboration from their project team, including Jason Etuangat, Rachel Mandel, and Robert Cooke.

## 8 References

- ASHRAE. (2009). *ASHRAE Handbook: Fundamentals*. Atlanta: American Society of Heating, Refrigerating and Air-Conditioning Engineers, Inc.
- ASTM. (2019). *E779-19 Standard test method for determining air leakage rate by fan pressurization*. West Conshohocken: American Society for Testing and Materials.
- Berardi, U., & Naldi, M. (2017). The impact of the temperature dependent thermal conductivity of insulating materials on the effective building envelope performance. *Energy and Buildings*, 144, 262-275.
- Brown, M. D. (2018). *Simulation and Optimization of High-Penetration Wind and Solar Energy for the Canadian High Arctic Research Station*. Ottawa: Carleton University.
- Canadian Solar. (2018). *All-Black: CS6K-290|295|300MS*. Walnut Creek: Canadian Solar (USA), Inc.
- CCBFC. (2015). *National Building Code of Canada*. Ottawa: National Research Council of Canada.
- De Soto, W., Klein, S. A., & Beckman, W. A. (2006). Improvement and validation of a model for photovoltaic array performance. *Solar energy*, 78-88.
- Duffie, J. A., & Beckman, W. A. (2006). *Solar Engineering of Thermal Processes*. Hoboken: John Wiley & Sons.
- ECCC. (2021a). *Engineering Climate Datasets*. (Government of Canada) Retrieved May 31, 2018, from Environment and Climate Change Canada: [https://climate.weather.gc.ca/prods\\_servs/engineering\\_e.html](https://climate.weather.gc.ca/prods_servs/engineering_e.html)
- ECCC. (2021b). *National Inventory Report 1990-2019: Greenhouse Gas Sources and Sinks in Canada: Part 2*. Gatineau: Environment and Climate Change Canada.
- EPA. (2019). *Greenhouse Gas Equivalencies Calculator*. Retrieved October 28, 2019, from U.S. Environmental Protection Agency: <https://www.epa.gov/energy/greenhouse-gas-equivalencies-calculator>
- Genie. (2017). *Product Selection - How fast will the garage door opener lift the door?* (The Genie Company) Retrieved January 13, 2022, from [https://overheaddoor.custhelp.com/app/answers/detail/a\\_id/1226/~product-selection---how-fast-will-the-garage-door-opener-lift-the-door%3F](https://overheaddoor.custhelp.com/app/answers/detail/a_id/1226/~product-selection---how-fast-will-the-garage-door-opener-lift-the-door%3F)
- Hatz Diesel. (2020). *Data sheet B-series*. Ruhstorf an der Rott: Motorenfabrik Hatz GmbH & Co. KG.
- ICC-SWCC. (2019). *ICC-SWCC Summary Report SWCC-11-04*. Brea: Small Wind Certification Council.
- ISED. (2018). *Volume correction factors—diesel, bio-diesel and diesel blends*. Retrieved January 11, 2022, from Innovation, Science and Economic Development Canada: <https://www.ic.gc.ca/eic/site/mc-mc.nsf/eng/lm00127.html>
- Klein, S. A., Cooper, P. I., Freeman, T. L., Beekman, D. M., Beckman, W. A., & Duffie, J. A. (1975). A method of simulation of solar processes and its application. *Solar Energy*, 29-37.
- Makaveckas, T., Bliūdžius, R., & Burlingis, A. (2021). Determination of the impact of environmental temperature on the thermal conductivity of polyisocyanurate (PIR) foam products. *Journal of Building Engineering*, 41.

- Mitalas, G. P., & Arseneault, J. G. (1972). *FORTTRAN IV Program to Calculate z-Transfer Functions for the Calculation of Transient Heat Transfer Through Walls and Roofs*. Ottawa: National Research Council Canada.
- Northern Container. (2022). *Shipping Container Dimensions: Internal and External Intermodal Container Dimensions*. Retrieved January 12, 2022, from <https://northerncontainersales.ca/more-info/container-dimensions/>
- NRCan. (2012). *R-2000 Standard*. Ottawa: Natural Resources Canada.
- QEC. (2017). *2018/19 General Rate Application*. Baker Lake: Qulliq Energy Corporation.
- SimpliPhi Power. (2022). Retrieved January 12, 2022, from PHI 3.8-M™ BATTERY: <https://simpliphipower.com/product/phi-3-8-m-battery/>
- Stephenson, D. G., & Mitalas, G. P. (1971). Calculation of Heat Conduction Transfer Functions for Multi-Layer Slabs. *ASHRAE Annual Meeting* (pp. 22-25). Washington: ASHRAE.
- TESS. (2019a). *TRNSYS: Transient System Simulation Tool*. Retrieved January 12, 2022, from <http://www.trnsys.com/>
- TESS. (2019b). *Trnsys 18 a TRaNsient SYstem Simulation program: Volume 4 - Mathematical Reference*. Madison: Thermal Energy System Specialists, LLC.
- TESS. (2019c). *Trnsys 18 a TRaNsient SYstem Simulation program: Volume 5 - Multizone Building modeling with Type56 and TRNBuild*. Madison: Thermal Energy System Specialists, LLC.
- Wills, A. D., Banister, C. J., & Berquist, J. (2019). *Detailed modelling of Cambridge Bay 8-plex and Renewable Energy Systems*. Ottawa: National Research Council Canada.